
ScienceDirect
Journals & Books
Help
Search
My account
Sign in
Access through your institution
Purchase PDF
Article preview
Abstract
Introduction
Section snippets
References (25)
Cited by (1)
Journal of Alloys and Compounds
Development of ODS tungsten heavy alloys reinforced with Co9Al8W superalloy binder by mechanical alloying
Chun-Liang Chen
Department of Materials Science & Engineering, National Dong Hwa University, Shou-Feng, Hualien 97401, Taiwan
Department of Mechanical Engineering, Institut Teknologi Nasional, Yogyakarta 55281, Indonesia
Received 6 October 2021, Revised 4 January 2022, Accepted 10 January 2022, Available online 15 January 2022, Version of Record 24 January 2022.
Recommended articles
Microstructural and mechanical characterization of tungsten containin...
Synthesis of ODS heavy tungsten alloys through post-annealing and secondary...
Effective joining between oxide dispersion strengthened tungsten-bas...
Show 3 more articles
FEEDBACK
Search
28°C Berawan

Journal of Alloys and Compounds 903 (2022) 163762

Contents lists available at ScienceDirect

Journal of Alloys and Compounds

journal homepage: www.elsevier.com/locate/jalcom

Development of ODS tungsten heavy alloys reinforced with Co9Al8W superalloy binder by mechanical alloying

Chun-Liang Chen[a,*], Sutrisna[a,b]

[a] Department of Materials Science & Engineering, National Dong Hwa University, Shou-Feng, Hualien 97401, Taiwan
[b] Department of Mechanical Engineering, Institut Teknologi Nasional, Yogyakarta 55281, Indonesia

ARTICLE INFO

Article history:
Received 6 October 2021
Received in revised form 4 January 2022
Accepted 10 January 2022
Available online 15 January 2022

Keywords:
Co-Al-W superalloy
Binder phase
Heavy tungsten alloys
Mechanical alloying

ABSTRACT

In the present study, the Co9Al8W superalloy was used as a binder phase for a new tungsten heavy alloy (WHA). The effects of the binder phase, nano-Y_2O_3 oxides, and mechanical alloying on the microstructure evolution and mechanical properties of the model WHAs were investigated. The results demonstrate that the presence of the Co9Al8W binder phase can stabilize the formation of solid phase during sintering. The dispersed oxide particles can interact with the Al element and form complex nanoscale Al-Y-O oxides, which greatly refine the microstructure, resulting in a significant impact on mechanical properties of the alloys. However, the porous microstructure related to Al-rich oxides and pores was obtained in the alloys, which caused the formation of micro-cracks, resulting in the loss of material ductility.

1. Introduction

Tungsten heavy alloys have superior properties including high density, high tensile strength, high ductility, high hardness, high absorption of radiation, and good wear resistance [1–4]. Therefore, they have been widely used in various industrial or medical applications such as kinetic energy penetrators, counterweight balance, radiation shields, and aerospace components [5–7]. WHAs are two-phase composites and the binder phases typically involve transition metals such as nickel, cobalt, iron, chromium, and copper, which are of great benefit for the ductility of WHAs. A new design of the binder phase is a critical issue for the enhanced performance of the next generation of WHAs. The binder phase with cobalt plays an important role in an increase of the strength and toughness at the interface between the binder phase and the tungsten matrix [8]. Thus, a new design of binder phases is essential for developing high performance WHAs. The use of high entropy alloys as a binder phase for heavy tungsten alloys has been recently studied and suggests that a fine-grained structure with improved mechanical properties can be achieved. [9,10].

In recent years, the Co-Al-W-based superalloy is considered to be the most promising candidate for high-temperature structural materials [11–13]. The formation of the stable $Co_3(Al,W)$ phase with $L1_2$ structure in the Co-Al-W ternary system discovered by Sato et al. [14] can dramatically enhance the thermal stability and strength at elevated temperatures. It would be expected that a novel design of the Co-Al-W alloy system used for a binder phase is an extremely attractive topic for the new development of WHAs. Thereby, in this study, the model WHAs with the Co9Al8W binder phase synthesized by mechanical alloying are investigated. The dispersed Y_2O_3 particles and the Mo element have been intentionally introduced in the model WHAs to promote the high-temperature mechanical properties by oxide dispersion strengthening and retard grain growth by solid solution strengthening of W and Mo [14]. This study aims to develop new WHAs with the Co9Al8W binder phase and understand how the binder phase and the oxide dispersoids influence the characteristics and sintering behavior of the model WHAs. It is also critical to discuss the interaction between the binder and the tungsten matrix.

2. Experimental methods

The materials used in this experiment were the W, Mo, Co, and Al element powders with an average particle size of 20–50 μm (purity > 99.9%). Yttrium oxide nanoparticles (~20 nm) were employed as dispersion strengthening for WHAs. Four kinds of model alloys were designed and named “W-B”, “W-B-YO”, “WMo-B”, and “WMo-B-YO”, see the composition of alloys listed in Table 1. A two-stage milling method was used for mechanical alloying. In the first stage, the Co-9Al-8W (at%) powders were pre-milled as a binder

* Correspondence to: No. 1, Section 2, Da Hsueh Rd., Shou-Feng, Hualien 97401, Taiwan.
E-mail address: chunliang@gms.ndhu.edu.tw (C.-L. Chen).

https://doi.org/10.1016/j.jallcom.2022.163762
0925-8388/

Table 1
The chemical composition of (a) the binder phase and (b) model alloys.

Binder phase (at%)			Co	Al	W
Co-Al-W			83	9	8
Model alloys (wt%)	W	Mo	Co-Al-W binder		Y_2O_3
W-B	90	–	10		–
W-B-YO	88	–	10		2
WMo-B	87	3	10		–
WMo-B-YO	85	3	10		2

phase for 24 h. The tungsten and the Co9Al8W binder powders were then further secondarily milled for 4 h, 8 h, 16 h, and 24 h. Mechanical alloying was performed in a high-energy planetary ball mill (Retsch PM100 instrument) with a rotational speed of 300 rpm under a highly pure argon atmosphere. The grinding media of tungsten carbide and a ball to powder weight ratio (BPR) of 10:1 was applied. A process control agent (stearic acid (0.5 wt%)) was used to avoid excessive cold welding and powder agglomeration during milling. The powder compact was consolidated by die-pressing at a pressure of 210 MPa in 15 s. The green compacted sample was sintered at 1450 °C for one hour under atmospheric pressure with a mixture of 10% hydrogen-90% argon. The chamber was pre-vacuumed before being purged in a protective atmosphere. Phase constituents were studied by X′Pert PRO XRD with CuKa radiation. Microstructure evolution, phase identification, and chemical composition of the model WHAs were examined using a Hitachi-4700 SEM and FEI Tecnai F20 G2 FEG-TEM equipped with EDS. Microhardness tests were conducted with a 1 kg load for 15 s at room temperature using a Vickers indenter. Nanoindentation experiments were carried out via an XP nanoindenter to obtain indentation hardness and elastic modulus. The maximum indentation depth and Poisson's ratio of the model WHAs were set to 2000 nm and 0.27, respectively. Compressive tests at room temperature were performed in a universal test machine with 100-kN capacity at a strain rate of 10^{-3} S^{-1}.

3. Results and discussion

3.1. Characterization of Co-9Al-8 W binder phase

3.1.1. XRD analysis of milled binder powders

Fig. 1 shows the XRD spectra of the Co9Al8W binder powders milled for 0 h, 4 h, 8 h, 16, and 24 h. The peaks of the Co and W elements were clearly identified in the XRD spectra of the un-milled powders; however, in this stage, the Al element shows a relatively weak peak at the low angle of 2θ around 39°. It is believed that the alloying element of tungsten has a high atomic number and thus its peak intensity is much stronger than that of Al and Co. After 8 h of milling, the Al peak was disappeared, suggesting the solid solution of Al into the Co matrix taking place during mechanical alloying. However, there is no solubility of tungsten in cobalt according to the binary phase diagram of the Co-W system [15] and thereby metastable Co-W intermetallic phases (eg. Co_7W_6, Co_3W) could be generated after a long milling time of 24 h as shown in Fig. 1.

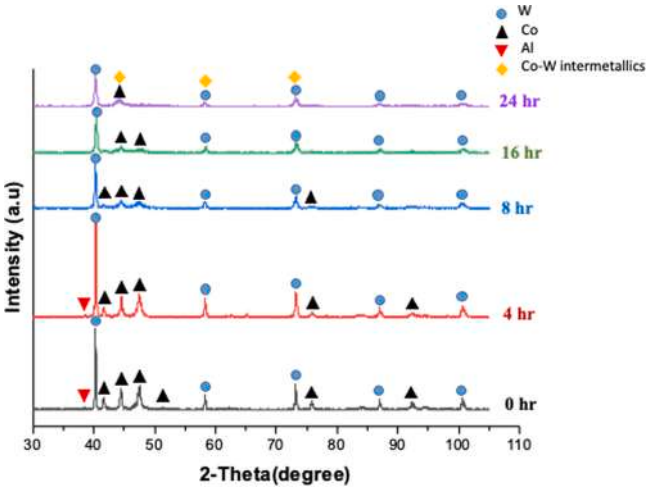

Fig. 1. XRD spectra of the Co9Al8W binder powders milled for 0 h, 4 h, 8 h, 16 h, and 24 h.

3.1.2. SEM-EDS analysis of sintered binder phase

Fig. 2 shows the microstructure development of the sintered Co9Al8W binder phase as a function of milling time. In the initial stage of milling (4 h), see Fig. 2a, the incomplete milling process causes the formation of W-rich / Al-rich particles, which are non-uniformly distributed in the Co matrix. After 8 h of milling, see Fig. 2b, the alloying element of W can interact with the Co matrix and forms Co-W intermetallic phases that appeared as a needle-like shape with a bright gray color. It has been reported that the needle-like Co_3W phase can be generated on the Co-Al-W-based superalloys [16]. Furthermore, the dark regions containing a high level of Al and O elements suggest the formation of Al-rich oxides promoted by the high-temperature sintering process. The needle-like Co-W phase was further refined and segregated with increasing the milling times to 16 h and 24 h (see Fig. 2c and d). The enlarged SEM image of the sintered Co9Al8W binder after 24 h of milling can be seen in Fig. 3a. The needle-like Co-W intermetallic phases tend to be embedded in the dark gray region where a high concentration of the Co, Al, and W elements was obtained. The EDS maps of Al and O also demonstrate the formation of Al-rich oxides (see Fig. 3b and c). In this case, the Al-rich oxide was preferable to form along the grain boundary where high energy and residual oxygen atoms can accelerate the diffusion and interaction of Al and O during high-temperature sintering.

3.2. Characterization of model WHAs

3.2.1. XRD analysis of milled WHA powders

Fig. 4 shows the XRD spectra of the tungsten powders (90 wt%) doped with the Co9Al8W binder powders (10 wt%) at different milling hours. In this case, the 24 h pre-milling of the Co9Al8W binder phase has been secondarily milled with the tungsten matrix powders. The results show that it is difficult to identify the Co9Al8W binder phase in the XRD spectra due to its small amount and the effect of high intensity from tungsten peaks. Hoverer, the broadening and shifting of reflection peaks were apparently observed with increasing milling time in the XRD spectra. It recommends that a longer mechanical alloying time can cause the increase of crystal imperfection and grain refinement of materials [17]. Strain energy associated with the crystal defects can promote the diffusion of the binder phase into the W matrix [18].

3.2.2. SEM-EDS investigation of sintered WHAs

Fig. 5 shows the microstructure development of the sintered WHAs with Co9Al8W binder phase at different milling times (4 h, 8 h, 16 h, and 24 h). In the initial milling times (4 h and 8 h), see Fig. 5a and b, the large binder phase appeared as a light gray area was clearly observed in the bright tungsten matrix. After long milling durations (see Fig. 5c and d), the Co9Al8W binder phase tends to be uniform and causes significant refinement of the microstructure. The small dark regions with porous microstructure were also found in the model alloy, which can be associated with the Al-rich oxides or pores, see Fig. 5d. It should be pointed out that during the high temperature sintering, the Al element is not sable and easily diffuses from the binder phase. The residual oxygen atoms between the milled powder particles can provide nucleation sites for the

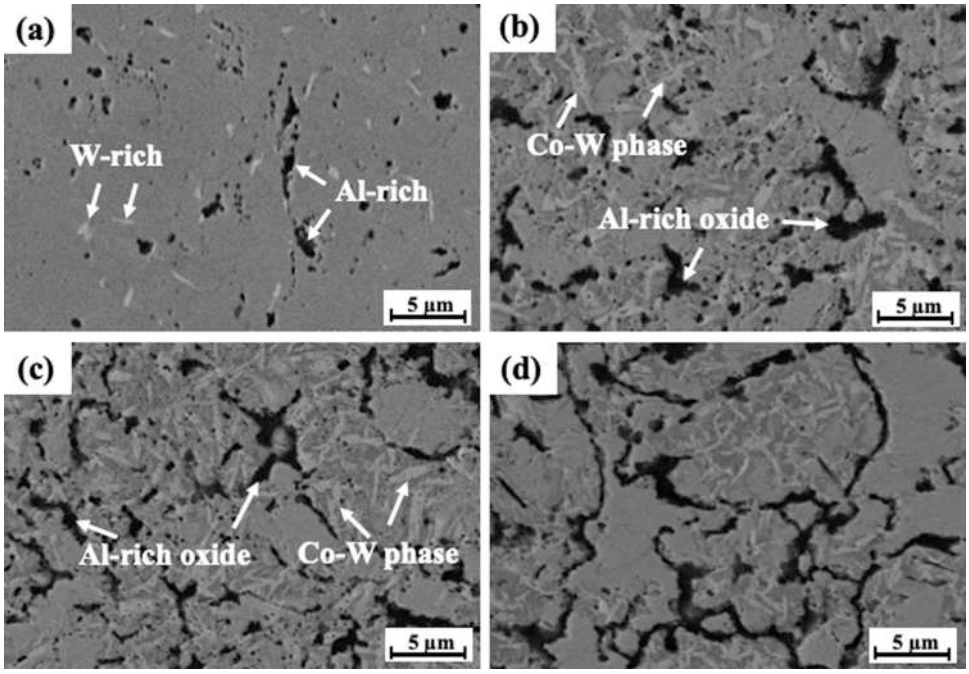

Fig. 2. SEM images of the sintered Co9Al8W binder phase after different milling times: (a) 4 h, (b) 8 h, (c) 16 h, and (d) 24 h.

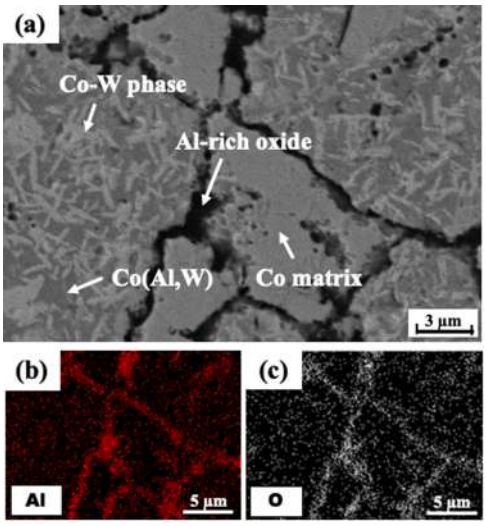

Fig. 3. (a) The enlarged SEM image of the sintered Co9Al8W binder phase after 24 h of milling; (b,c) The EDS maps of Al and O corresponding to Fig. 3(a).

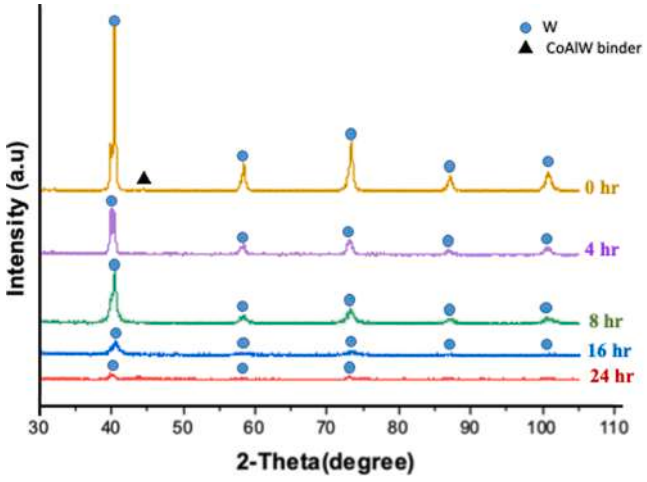

Fig. 4. XRD spectra of tungsten powders doped with Co9Al8W binder powders milled for 0 h, 4 h, 8 h, 16 h, and 24 h.

formation of Al-rich oxides surrounded by pores or binder phases. The high porosity of the alloy could be contributed to the sintering behavior, solubility and elemental diffusion between the binder and tungsten matrix. In this case, the use of the Co9Al8W binder phase in the WHAs can stabilize the formation of solid phase during sintering and also the high content of Co (83 at%) in the binder phase is insoluble to the tungsten matrix, which could cause a low fluidity and diffusion at the binder phase during sintering. Grain rearrangement and solution-reprecipitation do not take place in the WHAs and thus a large number of pores remain. Besides, the needle-like Co-W intermetallics observed in the Co-Al-W alloy system (see Fig. 2) were not found in the binder phase of the model alloy. The disappearance of the phase could be ascribed to two reasons. Firstly, a rapid interaction between the Co9Al8W binder phase and tungsten matrix was generated by high-energy ball milling, and subsequent high-temperature sintering results in a fast diffusion route for W atoms dissolved into the binder phase, impeding the formation ability of the complex Co-W intermetallic constituent. Secondly, the model alloy sintered at 1450 °C could cause phase decomposition, in this case, the Co-W intermetallic phase does not exist at such a high temperature according to the Co-W phase diagram [15].

Fig. 6 shows SEM micrographs and EDS analysis of the four model alloys after 24 h of milling. In the case of the W-B model alloy, see Fig. 6a, it exhibits a large grain structure and the Co9Al8W binder phase has a composition of 44.2Co-30.32Al-25.48 W (at%) as shown in the point "A", indicating the formation of the Co(Al,W) phase. The result reveals that the interaction between the tungsten and the binder phase affects the phase formation and microstructure development, which also promotes the formation of the solid phase during sintering. In addition, the pre-milling process of the Co9Al8W binder could lower its melting point in this alloy system and enhances the diffusivity. Thereby, a higher diffusion rate caused by elevated sintering temperature can encourage a high solubility of W and Al into the Co-based binder. The Al-rich oxide was also found in

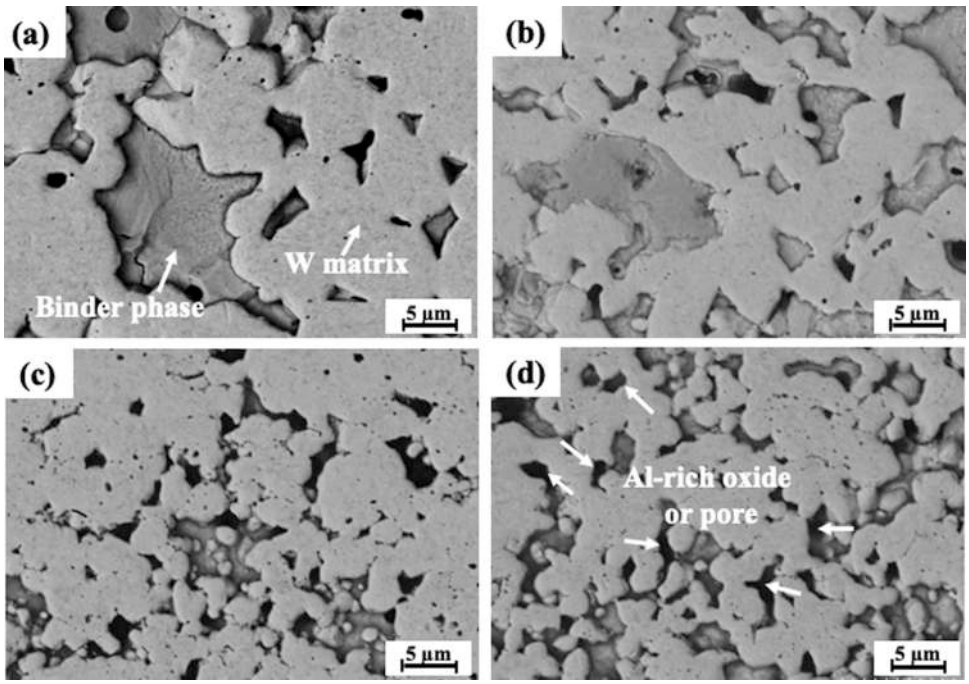

Fig. 5. SEM images of the W-B model alloy after different milling times: (a) 4 h, (b) 8 h, (c) 16 h, and (d) 24 h.

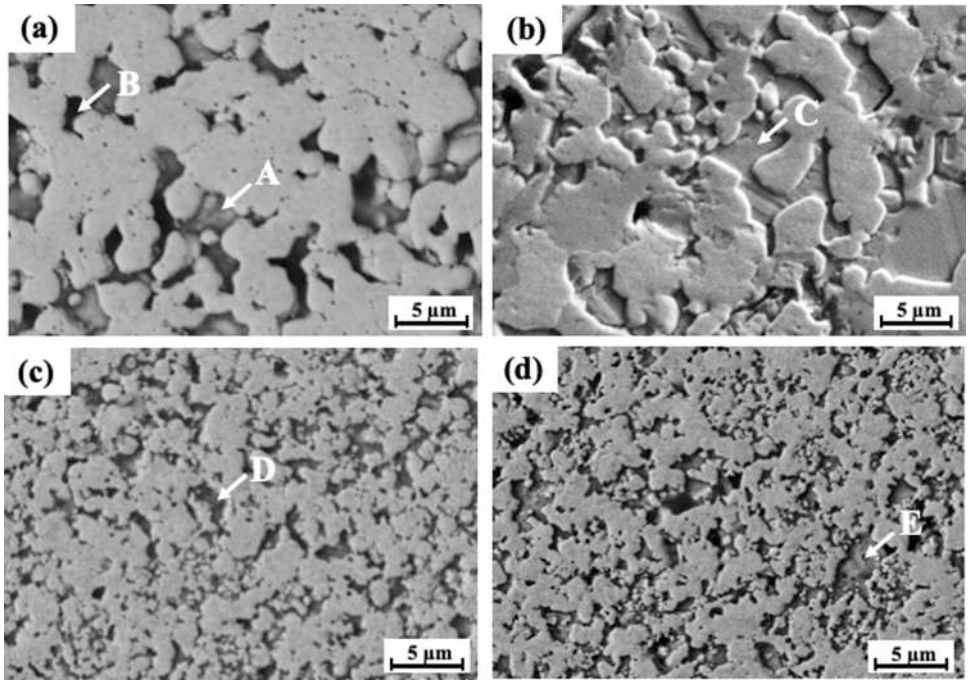

Fig. 6. SEM images of the four model WHAs (a) W-B, (b) WMo-B, (c) W-B-YO, (d) WMo-B-YO after 24 h of milling.

the alloy confirmed by EDS, see the point "B". Fig. 6b shows the SEM micrograph of the model WHA with the addition of Mo. It has been proposed that the presence of Mo in WHAs retards grain growth and facilities grain refinement [19]. However, in this study, grain coarsening was also observed in this sample and the microstructure has not been changed significantly in comparison to the Mo-free sample, see Fig. 6a. In this case, the Mo atoms tend to diffuse into the Co9Al8W binder phase, see the composition of the point "C", which could affect the refinement of the model WHAs. (Table 2)

Table 2
EDS analysis of the model alloys (at%) corresponding to Fig. 6.

Position	W	Mo	Co	Al	O
A (Fig. 6a)	25.48	–	44.20	30.32	–
B (Fig. 6a)	3.85	–	3.08	28.16	64.91
C (Fig. 6b)	38.50	2.79	44.25	14.45	–
D (Fig. 6c)	33.94	–	31.88	34.18	–
E (Fig. 6d)	44.49	4.42	40.52	10.57	–

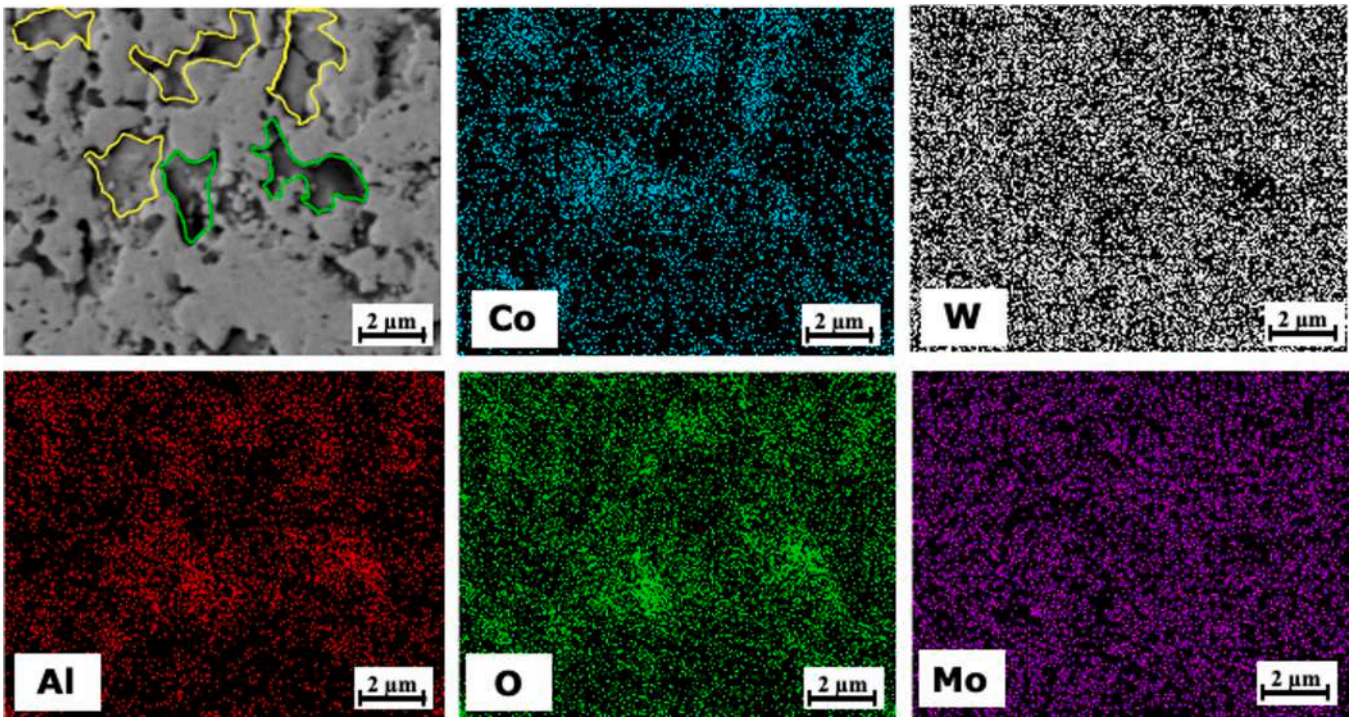

Fig. 7. EDS elemental maps showing the distribution of Co, W, Al, O, and Mo in the WMo-B-YO model alloy.

On the other hand, the model WHAs reinforced with the nano-oxide particles of Y_2O_3 have a pronounced effect on the microstructural features as shown in Fig. 6c and d. A homogeneous microstructure with a fine grain size was cleanly observed in the model alloys. It suggests that the addition of Y_2O_3 could act as a pinning force to inhibit the movement of grain boundary [16]. Furthermore, the sintering behavior can also be altered by doping with Y_2O_3 dispersoids, which provides an inhibitor for the diffusion of tungsten atoms at high-temperature sintering and facilitates the formation of solid-state sintering [14]. On the other hand, the presence of Mo does not lead to a significant change in microstructure in the case of the model alloys with the Y_2O_3 addition, see Fig. 6d. It recommends that the presence of Y_2O_3 dominates the formation of solid phase sintering, which has a strong effect on microstructure refinement.

A further investigation on distribution of individual elements was examined by EDS mapping analysis. Fig. 7. shows EDS maps of element distribution in the WMo-B-YO model alloy. It can be seen that the Co9Al8W binder phase is rich in cobalt (yellow line regions). EDS maps of Al and O also reveal the formation of Al-rich oxides (green line regions), which are the most frequently found near the binder phases where Al depletion and diffusion have taken place. W and Mo are uniformly distributed in the alloy.

3.2.3. XRD analysis and TEM observation of sintered WHAs

Fig. 8 shows the XRD spectra of the sintered model WHAs (W-B, W-B-YO, WMo-B, and WMo-B-YO). The strong peaks of the tungsten matrix have been identified. The enlarged region of XRD spectra at 2θ from 36° to 45° demonstrates the two small peaks corresponding to the Al oxide at ~ 38° and the Co9Al8W binder phase at ~43° detected in all model alloys. The results fit well with the correlation of SEM observation as shown in Fig. 6. The XRD result also indicates that the model alloys with the Mo addition have a lower intensity of

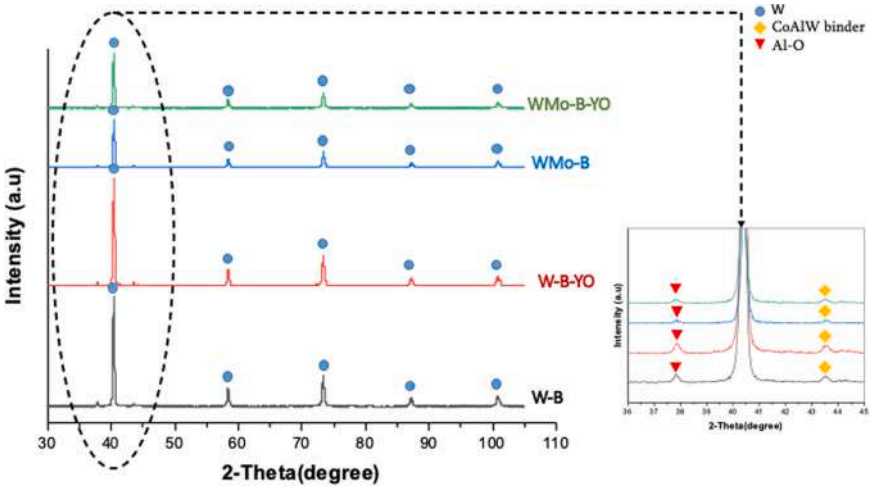

Fig. 8. XRD spectra of the four model WHAs.

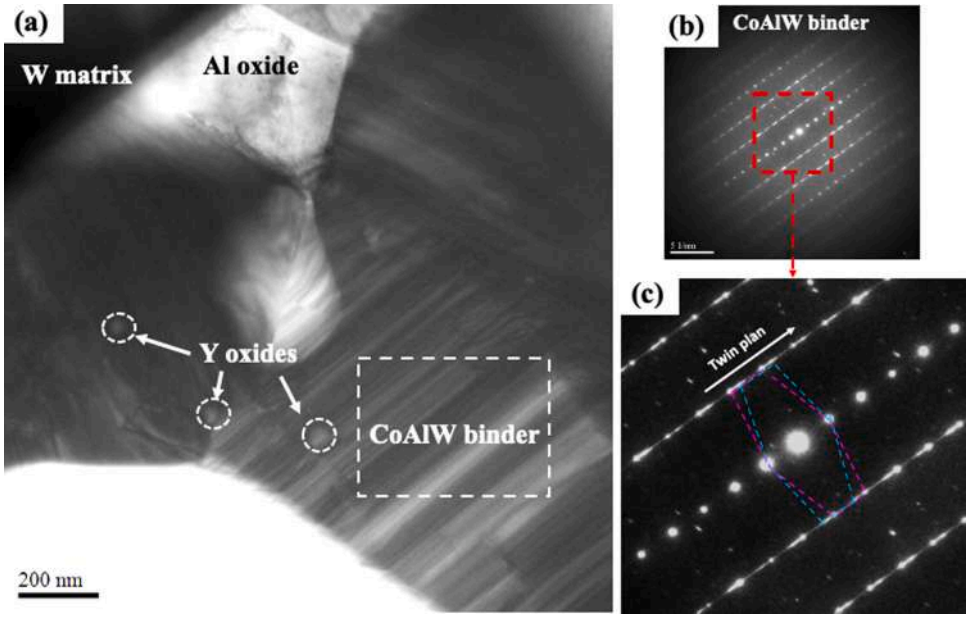

Fig. 9. TEM image of the WMo-B-YO model alloy.

tungsten peaks, see Fig. 8. It is believed that Mo can form a substitutional solid solution with the tungsten matrix during mechanical alloying [20], which causes crystallographic defects due to the imperfection in crystals, leading to a decrease of peak intensity. Fig. 9a shows the TEM image of the model WHA dispersed with the Y_2O_3 addition and the different phases were observed by the varied contrasts and structures. The region with a high concentration of Co, W, and Al elements corresponding to the binder phase was investigated. It can be seen apparently that the twinned structure was found in the Co9Al8W binder phase as shown in Fig. 9c of the enlarged SAED pattern. It has been reported that relatively low stacking fault energies (SFE) were observed in Co-base γ' and $\gamma + \gamma'$ alloys [21]. In this case, the pre-milling of the Co-based binder with the low SFE can promote the deformation twins subjected to severe plastic deformation by mechanical alloying process.

Furthermore, the result also demonstrates that the Y-rich oxide particles with nanoscale dimensions (~30 nm) containing a high level of Y, Al, and O elements were revealed in the model alloy. It recommends that the nano-Y_2O_3 oxide particles can act as favorable nucleation sites to promote the formation of complex oxide particles by solid-state interacting with the Al element from the Co9Al8W binder phase during ball milling. It has been reported that complex Al-Y-O oxide dispersoids such as $Y_4Al_2O_9$ (YAM), $YAlO_3$ (YAP), and $Y_3Al_5O_{12}$ (YAG) can be generated by mechanical alloying in the Al-containing alloys with the nano-Y_2O_3 addition [22,23]. In this study, the presence of Al-Y-O oxide is important to the microstructure development, mechanical properties, and sintering behavior of WHAs.

3.3. Mechanical properties of sintered WHAs

3.3.1. Microhardness

Fig. 10a shows the microhardness measurements of the WMo-B-YO model alloy at different milling times. The result indicates that the hardness values increase with increasing milling time from 455.1HV for 4 h of milling to 624.2HV for 24 h of milling. It can be attributed that the distribution of the Co9Al8W binder phase was not uniform at the initial stages of milling; however, homogeneous microstructure, grain refinement, and high work hardening can be achieved by a long milling time.

Fig. 10b shows the microhardness results of the four model WHAs milled for 24 h. The high hardness values (615.2 HV and 624.2 HV) were obtained in the samples adding with the oxide dispersoids. Obviously, the presence of Y_2O_3 does not only refine the binder

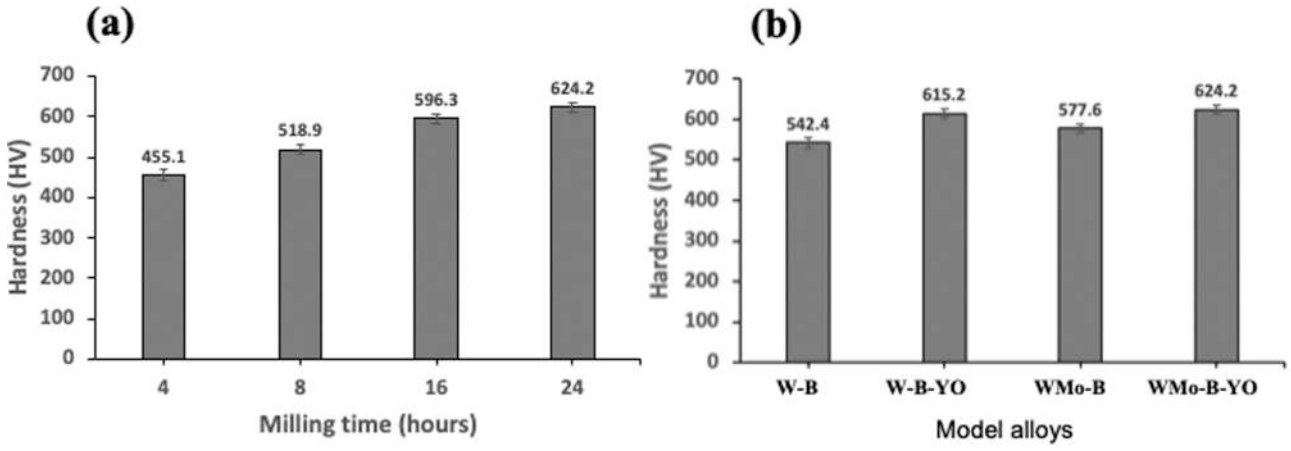

Fig. 10. (a) The microhardness of the WMo-B-YO model alloys at different milling durations and (b) the microhardness of the four model WHAs.

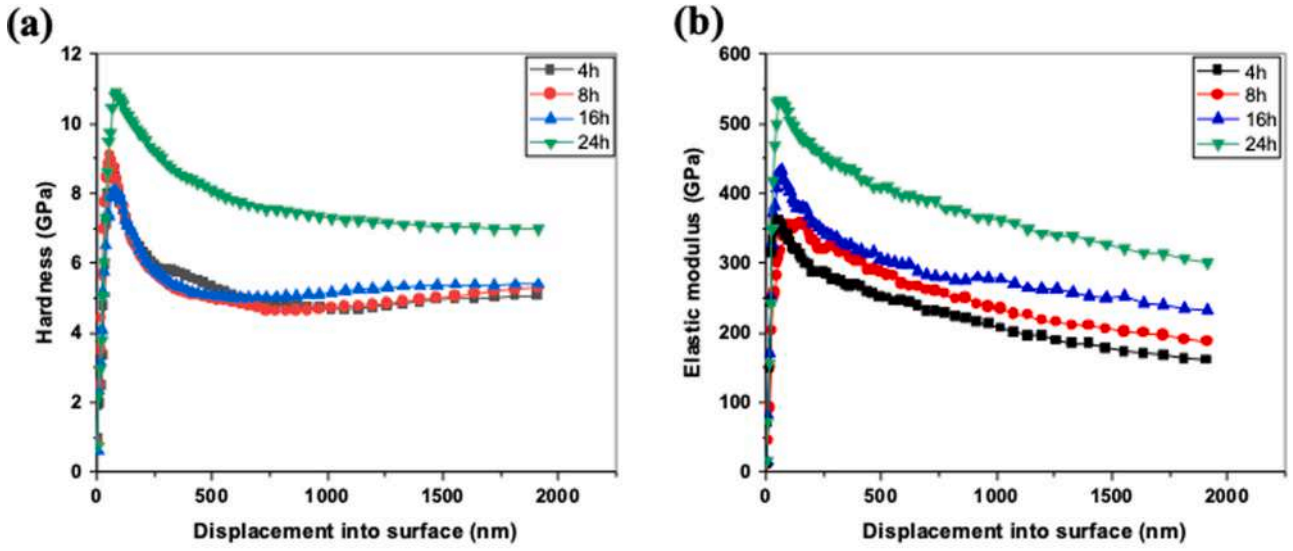

No	Milling time (hours)	Hardness (GPa)	Elastic modulus (GPa)
1	4	5.34±0.27	326.92±7.73
2	8	5.51±0.26	335.59±7.46
3	16	5.92±0.26	346.41±7.37
4	24	8.76±0.24	425.37±7.34

Fig. 11. Nanoindentation measurements of the WMo-B-YO model alloys at different milling durations: (a) hardness and (b) elastic modulus.

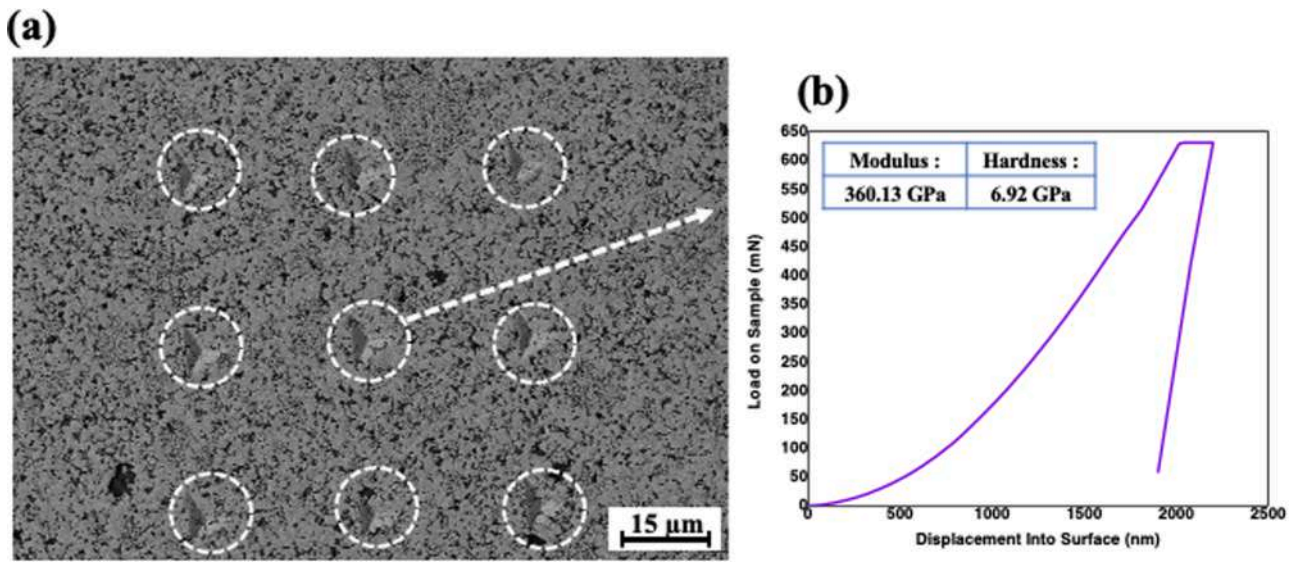

Fig. 12. (a) SEM image of nanoindentation indents and (b) a typical load-displacement curve of the WMo-B-YO model alloy.

phase and tungsten grains but also alters the sintering behavior, which has a strong tendency to the formation of solid-phase sintering.

Moreover, the number of complex Al-Y-O nano-oxides were embedded into the tungsten matrix and impedes the grain coarsening, which also contributed to the increase in hardness. In our earlier study [14], the W-Mo alloy reinforced with the conventional binder phase (70Ni-15Fe-15Co wt%) was investigated and has the microhardness value of 364 HV, which is much lower than that of using the Co9Al8W binder phase in this study (577.6 HV). This can be attributed to the Co9Al8W binder which provides the opportunity of achieving a combination of high strength and ductility associated with the formation of superlattice structure. Furthermore, it should be noted that Al and Y elements are not stable at high temperatures and tend to form Al-rich oxides or complex nano Al-Y-O dispersoids, which can provide dispersion strengthening for improvement of mechanical properties.

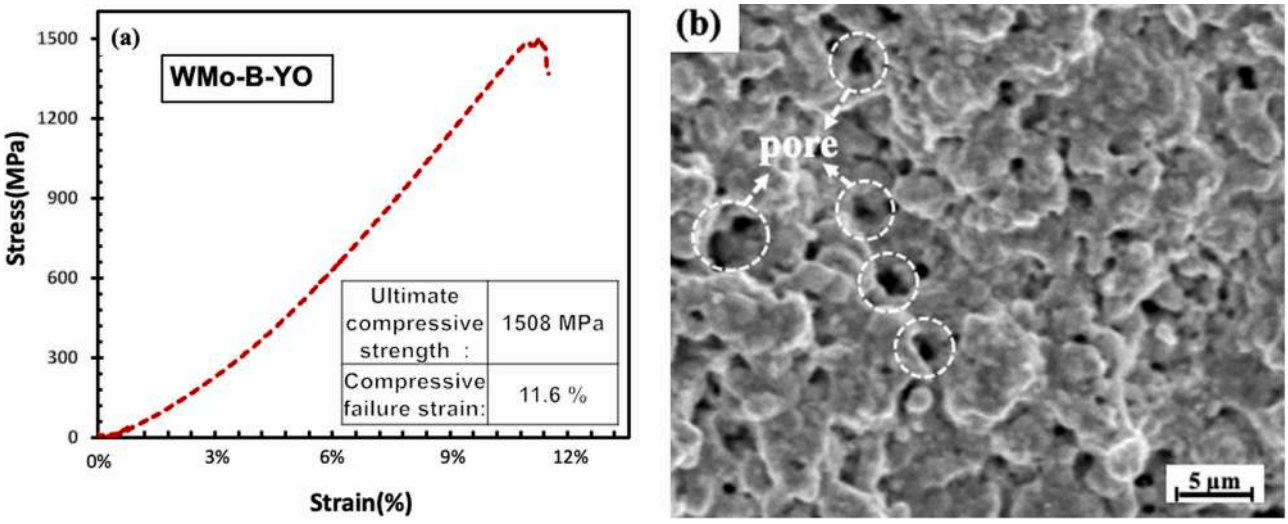

Fig. 13. (a) Engineering stress-strain curve and (b) fracture surface of the WMo-B-YO sample at room temperature by compression test.

3.3.2. Nanoindentation

Nanoindentation was further used to determine the hardness and elastic modulus of the model WHAs. Fig. 11 shows the curves of hardness-displacement and modulus-displacement of the WMo-B-YO model alloy at different milling durations. It can be observed that a considerable increase in the hardness and elastic modulus was achieved after 24 h of milling. In the present study, it should be also careful about the indentation size effect [24], which exhibits an increase in the hardness and elastic modulus with decreasing indentation depth as shown in Fig. 11. The SEM image with 9 indentations and a typical load-displacement curve of the sample is shown in Fig. 12a and b. It indicates that the long milling duration is important to facilities the microstructure homogeneity, densification, and refined grain size of the Co9Al8W binder.

3.3.3. Compression testing

The microhardness and nanoindentation tests only provide local properties of the alloys. Therefore, the compression tests were further performed on the sample of WMo-B-YO, which has a uniform fine-grained structure with the highest hardness value. Fig. 13a shows the engineering stress-strain of the model alloy by compression test. The ultimate compressive strength of 1508 MPa was determined, which exhibits higher strength compared to the conventional tungsten heavy alloy (90 W-7Ni-3Fe) with UCS of 1150 MPa [25]. However, the low compressive failure strain of 11.6% was obtained, which can be attributed to the formation of porous microstructure in the model alloy. Fig. 13b also shows the fracture surface of the failed compression specimen and reveals that a large number of pores were surrounded by a fine-grained structure of the tungsten matrix or binder phases. The initiation and propagation of micro-cracks were mainly caused by the stress concentration that occurred from the pores. Thus, the presence of numerous pores segregated with Al-rich oxides can deteriorate the capacity to resist plastic deformation of the alloys, resulting in the loss of material ductility.

4. Conclusions

In the present study, the new tungsten heavy alloys doped with the Co9Al8W binder phase were produced by mechanical alloying. The effects of the Co9Al8W binder phase and dispersed oxide particles on the characteristics and mechanical properties of the model WHAs were investigated. The results indicate that the pre-milling of the Co9Al8W binder phase causes the formation of the needle-like Co-W intermetallic phases. The addition of the Co9Al8W binder phase can stabilize the formation of solid phase during sintering, which could provide a high heat resistance for enhanced thermal stability to the materials. The Y_2O_3 oxide particles can interact with Al from the binder phase during ball milling. Therefore, complex nano-Al-Y-O oxides can be generated. The presence of nano-dispersed oxide particles can further promote a homogeneous microstructure with fine grain size, leading to a significant increase in hardness and compressive strength. However, the porous microstructure associated with the Al-rich oxides and pores was found in the model alloys, which can deteriorate the capacity to resist plastic deformation of the alloys and causes low ductility.

CRediT authorship contribution statement

Chun-Liang Chen: Methodology, Supervision, Writing – original draft, Conceptualization, Validation, Writing – review & editing, Resources, Project administration. **Sutrisna:** Methodology, Software, Data curation, Visualization, Writing – original draft, Investigation.

Declaration of Competing Interest

The authors declare that they have no known competing financial interests or personal relationships that could have appeared to influence the work reported in this paper.

Acknowledgments

The authors would like to gratefully acknowledge financial support from Ministry of Science and Technology (MOST) Taiwan under the grant MOST 108-2221-E-259-017-MY2 and MOST 110-2221-E-259-012-MY2.

References

[1] O. Dinçer, M.K. Pehlivanoılu, N.K. Çalişkan, I. Karakaya, A. Kalkanli, Processing and microstructural characterization of liquid phase sintered tungsten-nickel-cobalt heavy alloys, Int. J. Refract. Met. Hard Mater. 50 (2015) 106–112, https://doi.org/10.1016/j.ijrmhm.2014.12.009

[2] Y. Şahin, Recent progress in processing of tungsten heavy alloys, J. Powder Technol. 2014 (2014) 764306–764322, https://doi.org/10.1155/2014/764306

[3] A. Arora, V.Gopal Rao, Tungsten heavy alloy for defence applications, Mater. Technol. 19 (2004) 210–215, https://doi.org/10.1080/10667857.2004.11753087

[4] R.M. German, K.S. Churn, Sintering atmosphere effects on the ductility sintering atmosphere effects on the ductility of W-Ni-Fe heavy metals, Metall. Trans. A 15 (1984) 747–754, https://doi.org/10.1007/BF02644206

[5] K.H. Lee, S.I. Cha, H.J. Ryu, S.H. Hong, Effect of two-stage sintering process on microstructure and mechanical properties of ODS tungsten heavy alloy, Mater. Sci. Eng. A 458 (2007) 323–329, https://doi.org/10.1016/j.msea.2007.01.118
[6] A. Upadhyaya, S.K. Tiwari, P. Mishra, Microwave sintering of W-Ni-Fe alloy, Scr. Mater. 56 (2007) 5–8, https://doi.org/10.1016/j.scriptamat.2006.09.010
[7] W.S. Lee, S.T. Chiou, The influence of loading rate on shear deformation behaviour of tungsten composite, Compos. Part B Eng. 27 (1996) 193–200, https://doi.org/10.1016/1359-8368(95)00051-8
[8] L. Zhang, X. Qu, X. He, R.U. Din, H. Liu, M. Qin, H. Zhu, Microstructural characterization of co-based ODS alloys, J. Mater. Eng. Perform. 21 (2012) 2487–2494, https://doi.org/10.1007/s11665-012-0206-3
[9] P.V. Satyanarayana, R. Sokkalingam, P.K. Jena, K. Sivaprasad, K.G. Prashanth, Tungsten matrix composite reinforced with CoCrFeMnNi high-entropy alloy: impact of processing routes on microstructure and mechanical properties, Metals 9 (2019) 992, https://doi.org/10.3390/met9090992
[10] C.-L. Chen, Sutrisna, Study of NiFeCoCr medium entropy alloy as a binder phase on W–Mo heavy tungsten alloy by secondary ball milling, Intermetallics 138 (2021) 107320, https://doi.org/10.1016/j.intermet.2021.107320
[11] M. Cartón-Cordero, B. Srinivasarao, M. Campos, A. García-Junceda, J.M. Torralba, On the role of processing parameters in sintered new Co-based (W,Al) alloys, J. Alloy. Compd. 674 (2016) 406–412, https://doi.org/10.1016/j.jallcom.2016.03.077
[12] H.-Y. Yan, V.A. Vorontsov, D. Dye, Alloying effects in polycrystalline γ' strengthened Co-Al-W base alloys, Intermetallics 48 (2014) 44–53, https://doi.org/10.1016/j.intermet.2013.10.022
[13] J. Sato, T. Omori, K. Oikawa, I. Ohnuma, R. Karinuma, K. Ishida, Cobalt-base high-temperature alloys, Science 312 (2006) 90–91, https://doi.org/10.1126/science.1121738
[14] C.-L. Chen, Sutrisna, The effect of Mo and dispersoids on microstructure, sintering behavior, and mechanical properties of W-Mo-Ni-Fe-Co heavy tungsten alloys, Metals 9 (2019) 111–8331, https://doi.org/10.3390/met9020111
[15] H. Okamoto, M.E. Schlesinger, E.M. Mueller, Alloy phase diagrams, ASM HANDBOOK, ASM Int. 3 (2016) ISBN electronic: 978-1-62708-163-4.
[16] C.L. Chen, Suprianto, Influence of Ta and Y2O3 on synthesis, phase evolution and mechanical properties of Co-Al-W based alloys, J. Alloy. Compd. 791 (2019) 567–574, https://doi.org/10.1016/j.jallcom.2019.03.262
[17] C. Suryanarayana, E. Ivanov, V.V. Boldyrev, The science and technology of mechanical alloying, Mater. Sci. Eng. 304-306 (2001) 151–158, https://doi.org/10.1016/S0921-5093(00)01465-9
[18] C. Suryanarayana, Mechanical alloying and milling, Prog. Mater. Sci. 46 (2001) 1–184, https://doi.org/10.1016/S0079-6425(99)00010-9
[19] C.S. Hsu, S.T. Lin, Effect of molybdenum on grain growth of W-Mo-Ni-Fe heavy alloys, J. Mater. Sci. 38 (2003) 1543–1549, https://doi.org/10.1023/A:1022941119017
[20] C.-L. Chen, Sutrisna, Study of NiFeCoCr medium entropy alloy as a binder phase on W–Mo heavy tungsten alloy by secondary ball milling, Intermetallics 138 (2021) 107320, https://doi.org/10.1016/j.intermet.2021.107320
[21] A. Suzuki, H. Inui, T.M. Pollock, L12-strengthened cobalt-base superalloys, Annu. Rev. Mater. Res. 45 (2015) 345–368, https://doi.org/10.1146/annurev-matsci-070214-021043
[22] C.H. Zhang, A. Kimur, R. Kasada, J. Jang, H. Kishimoto, Y.T. Yang, Characterization of the oxide particles in Al-added high-Cr ODS ferritic steels, J. Nucl. Mater. 417 (2011) 221–224, https://doi.org/10.1016/j.jnucmat.2010.12.063
[23] C.L. Chen, G.J. Tatlock, A.R. Jones, Effect of annealing temperatures on the secondary re-crystallization of extruded PM2000 steel bar, J. Microsc. 233 (2009) 474–481, https://doi.org/10.1111/j.1365-2818.2009.03134.x
[24] G.M. Pharr, E. Herbert, Y. Gao, The indentation size effect: a critical examination of experimental observations and mechanistic interpretations, Annu. Rev. Mater. Res. 40 (2010) 271–292 doi:10.1146/annurev-matsci-070909-104456. ISSN 1531-7331.
[25] Y. Yu, C. Ren, W. Zhang, Compressive behavior of liquid phase sintered 90W–7Ni-3Fe heavy alloy at high temperature and low strain rate condition, Int. J. Refract. Met. Hard Mater. 76 (2018) 149–157, https://doi.org/10.1016/j.ijrmhm.2018.06.006